scientific reports

Check for updates

OPEN

Simplistic metasurface design approach for incident angle and polarization insensitive rcs reduction

K. K. Indhu[1]✉, A. P. Abhilash[1], R. Anilkumar[1], Deepti Das Krishna[1] & C. K. Aanandan[2]

This paper proposes the design of a metasurface for polarization and incident angle-insensitive RCS reduction applications. An ellipse-shaped unit cell is utilized as a polarization converter, which is then arranged to form a checkerboard surface. While a single layer checkerboard structure gives a wideband RCS reduction, a double layer structure yields polarization and incident angle independent operation. The two layers have unit cells rotated 45^0 to each other. Experimental results demonstrate an RCS reduction bandwidth of around 90%. Further the RCS reduction remains stable with polarization and incident angle variation.

Keywords Polarisation insensitive, Incident angle stability, Radar cross section reduction, Polarisation conversion ratio, Checker board reflective surface

Reducing the radar cross-section (RCS) is an integral part of safeguarding assets, augmenting military efficacy, and maintaining a strategic advantage in modern warfare. Research is ongoing to develop and improve techniques for RCS reduction[1]. The manipulation of electromagnetic wave polarization with metasurfaces has emerged as an effective way to reduce RCS, and it has garnered significant interest. Smith et al.[2] introduced metamaterials, which are man-made substances with unique properties. These materials consist of subwavelength-sized electric & magnetic resonators arranged in a periodical structure. Metasurfaces are the 2-dimensional and planar version of metamaterials that have several advantages, including compactness and seamless integration with devices. Metasurfaces have shown promise as polarization converters[3–8]. Polarization Conversion Metasurfaces (PCM) have garnered considerable attention in RCS reduction applications, like in antenna[9–12] and target structural RCS reduction[13–20]. They transform incident waves into cross-polarized waves, leading to scattering wave cancellation. Unlike approaches utilizing multiple unit cell types[21–26], arranging a single type of PCM in checkerboard configuration can effectively reduce RCS across a wide bandwidth[9–20]. Another approach for reducing RCS is by using coding metasurfaces[27–35]. Coding metamaterials and digital metamaterials have potential to regulate the scattered electromagnetic waves by using designs that incorporate code sequences of "0" and "1". This approach enables different functions like abnormal reflection, polarisation conversion, scattering beams diffusion, all contributing to achieving low RCS. In the existing literature, polarization conversion has been observed to be affected by both incident angles and the polarization of the incident waves. However, several studies have been conducted to explore designs that are insensitive to polarization and angle, as reported in[36–41]. While some researchers, have reported an incident angle-insensitive polarization rotator, they have not carried out RCS analysis[36–38]. Recently, Liu et al. proposed a novel approach for designing polarization-insensitive and angle-stable response[39]. Other studies[40,41,46–48] have also reported achieving RCS reduction in a wide bandwidth using symmetrical metasurfaces that exhibit polarization and incident angle independence. In[41], they achieved polarization and angle insensitivity using a symmetrically optical transparent metasurface, which resulted in broadband mono and bi-static RCS reduction with a bandwidth of 61.5%. In the reported works, resonating elements of different size are utilised to achieve multiple resonances which increases the number of parameters in the design.

In this paper, we present the design of an array based on simple elliptical structure to reduce radar cross-section (RCS) over a wide bandwidth. The RCS reduction achieved is insensitive to incident polarization and angle of incidence. We first evaluate a polarization rotation surface and then a conventional checkerboard

[1]Department of Electronics, Cochin University of Science and Technology, Cochin 682022, India. [2]Advanced Centre for Atmospheric Radar Research, Cochin University of Science and Technology, Cochin 682022, India. ✉email: indhukk@cusat.ac.in

arrangement for RCS reduction. To achieve polarization insensitivity, we use a double-layer structure. The top layer has ellipses arranged in a checkerboard pattern with + 45 and −45° orientations. The bottom layer has ellipses arranged in 0° and 90° orientations, with a ground on the back side.

Design of PCM unit cell

The suggested unit cell, elliptical in shape, is fabricated on a single-layer, 3.2 mm thick FR4 substrate with ε_r and 'tan δ' being of 4.3, and 0.02, respectively. The choice of substrate thickness was indeed a critical design parameter. A thicker substrate was selected to support the broader bandwidth and to ensure sufficient structural rigidity[49,50]. There is a trade-off between the substrate thickness and the operational bandwidth, with thicker substrates generally enabling broader bandwidths at the cost of increased weight and potential manufacturing complexity. To rotate the vertically or horizontally polarized incident electric field, the ellipse structure is diagonally aligned. Unit cell is stimulated in CST by a Floquet port excitation. The optimised geometry of the elliptical unit cell with ground plane is depicted in (Fig. 1).

The polarization rotation of a surface can be determined by analysing the response to the incoming electromagnetic radiation. This assessment involves analysing the response of the meta-surface to the incoming radiation. The polarization conversion ratio (PCR) of the polarisation rotation reflective surface (PRRS) can be estimated[42] as,

$$PCR = \frac{|r_{xy}|^2}{|r_{xy}|^2 + |r_{yy}|^2} \tag{1}$$

where in, $r_{xy} = \frac{|\rightarrow E_{rx}|}{|\rightarrow E_{iy}|}$ and $r_{yy} = \frac{|\rightarrow E_{ry}|}{|\rightarrow E_{iy}|}$ represent the reflection ratios for the y-to-x and y-to-y polarization rotations. Here, E_{iy} denotes electric field of the incident y-polarised electromagnetic wave, while E_{rx} and E_{ry} refers to the x- and y-polarised reflected waves, respectively. Figure 2 shows the simulated outcomes of r_{yy}, r_{xy} and the calculated PCR, for the unit cell. It is clear from the plots that the proposed unit cell design is a PRRS with almost 72% bandwidth (6.4 to 14 GHz), with the PCR consistently exceeding 90%. The polarization rotation bandwidth reaches 72%, spanning from 6.4 to 14 GHz, with the PCR consistently exceeding 90%.

In Fig. 3a, the y-polarised incident electric field, E_i, is separated as components, E_{iu} and E_{iv}, oriented along the u & v axis, respectively, along 45 and 135° angles from the x-axis. This decomposition allows for an examination of the PRRS behaviour[43]. The magnitude and phase of the reflected electric fields, E_{ru} and E_{rv}, are plotted in (Fig. 3c,d). Notably, the magnitudes of the reflected fields are nearly identical and their reflected phase disparity ($\Delta\varphi$) remains close to 180° across the frequency band from 6.4 to 14 GHz. Consequently, total reflected electric field, E_r, aligns parallel to x-axis in the + x direction and possesses the same magnitude as E_i. Hence E_r is perpendicular to E_i, thereby achieving a 90° polarization rotation. This is further confirmed by the reflection coefficients $r_{xy} = \sqrt{1 - \cos(\Delta\varphi/2} = 1$ and $r_{yy} = \sqrt{1 + \cos(\Delta\varphi)/2} = 0$ over the entire bandwidth. The structure in (Fig. 3b) which is mirror reflection of (Fig. 3a), gives a reflected field in the –x direction as depicted.

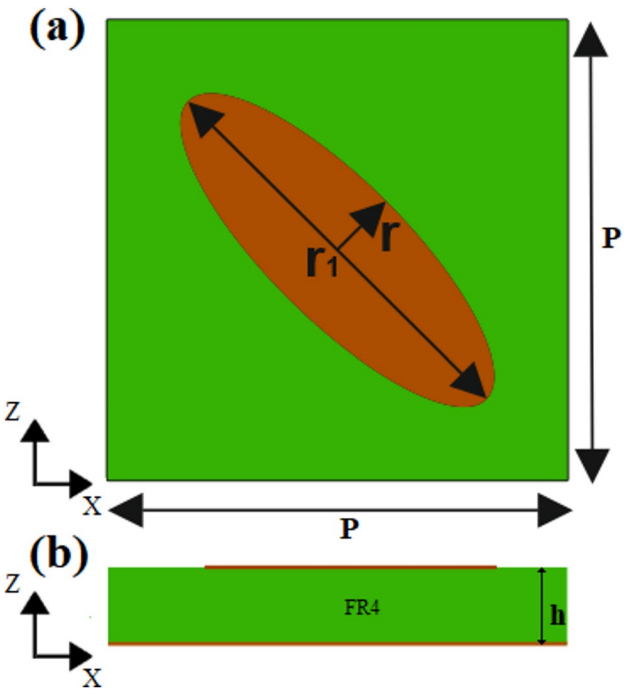

Fig. 1. The unit cell (**a**) top view (r = 1.8 mm, r_1 = 11 mm, P = 12 mm) (**b**) side view.

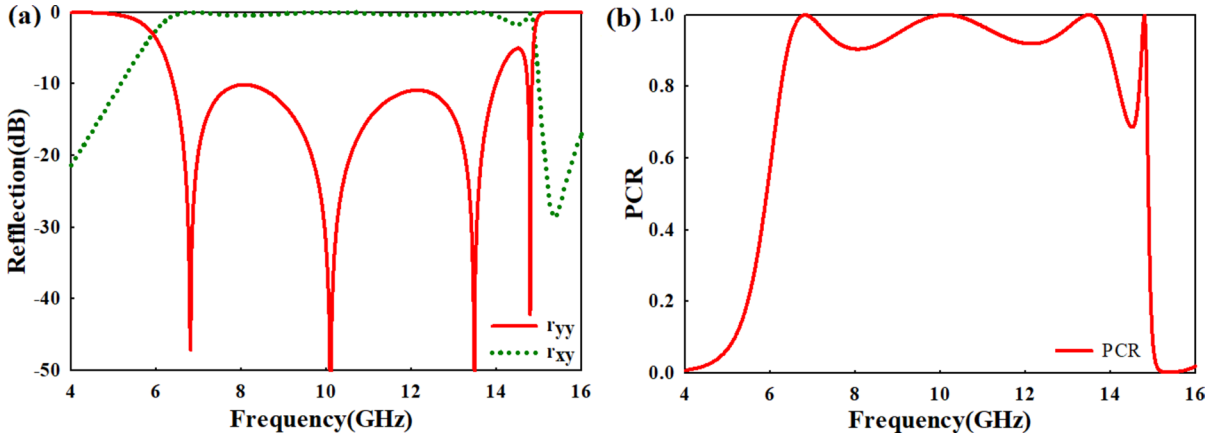

Fig. 2. Simulated results (**a**) r_{yy}, r_{xy} (**b**) PCR.

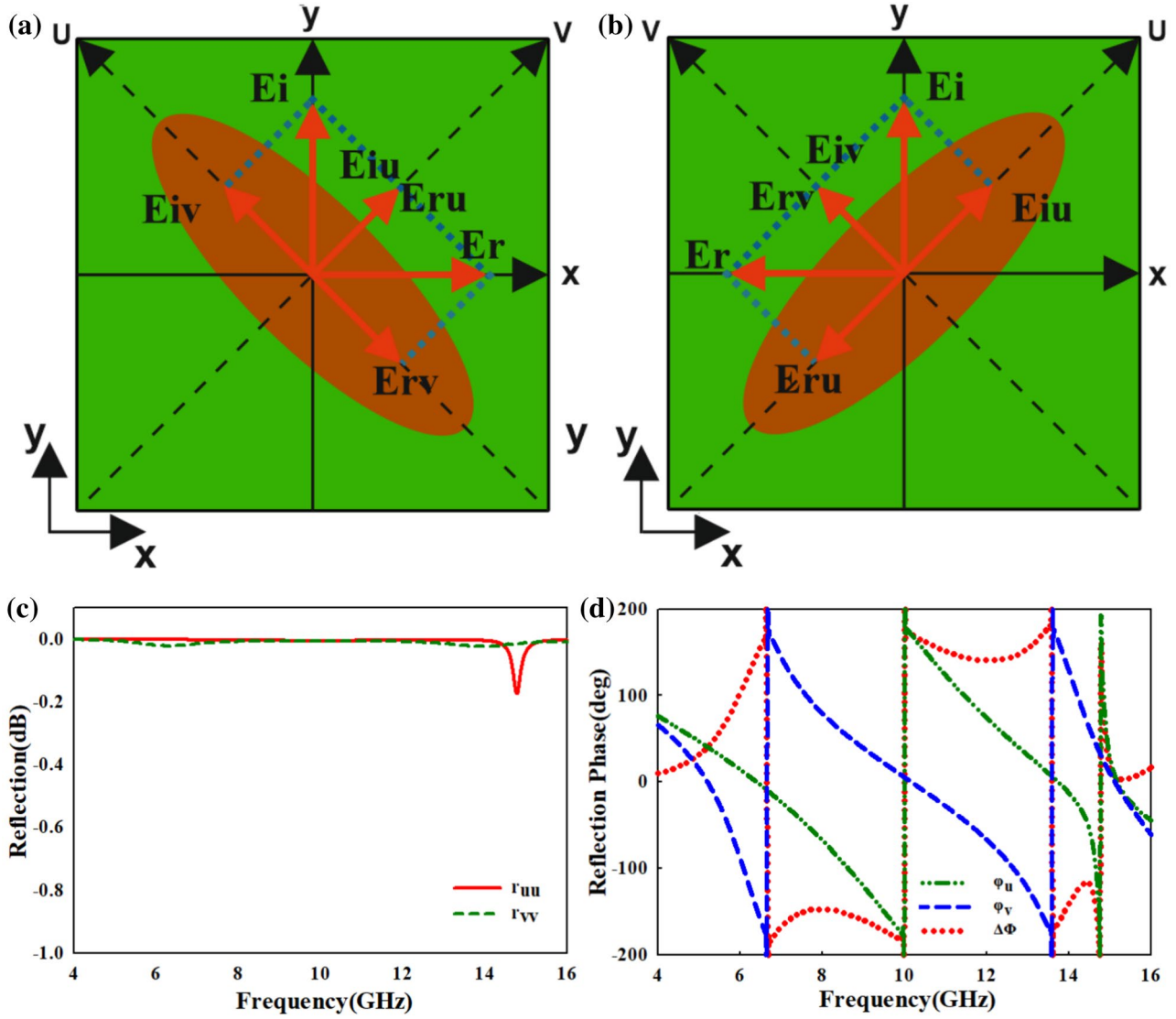

Fig. 3. Polarisation conversion for a normally incident y-polarised plane wave (**a**)135^0 ellipse converter (**b**) 45^0 ellipse (**c**) Reflection coefficient (**d**) Reflected phase disparity ($\Delta\varphi$).

To investigate the wideband polarization conversion, the current distribution on the top and bottom layers at the three resonant frequencies are plotted in (Fig. 4). The arrow indicates the direction of the current in the top layer and ground plane. At all the three frequencies, surface current on the unit cell trigger current on the ground plane. The orientation of these induced currents dictates the resonance category. Electric resonance occurs when the currents on the metallic unit cell's surface align in parallel with those generated on the ground plane. Conversely, when the surface current on the upper unit cell and induced current on the lower ground plane are oriented in opposite directions, creating loops of current, it leads to the magnetic resonance[44].

Fabrication and measurement

A photograph of 24 × 24 array of PRRS unit cell fabricated on an FR-4 substrate is depicted in (Fig. 5a). Measurement is conducted in an anechoic chamber utilizing a Keysight PNA N5227A network analyzer. Schematic diagram and the photograph of the measurement set up are depicted in (Fig. 5b,c). To ensure plane wave excitation, standard horn antennas (2–18 GHz) are placed at a far-field distance from the target. Time gating is employed to minimize residual reflection. The structure is positioned for normal incidence with the transmitting and receiving antenna kept side by side and calibrated using a PEC surface of identical size. The measured co-polarization, cross-polarization, and PCR of the intended PRRS array under normal incidence of 'y'-polarized EM waves are depicted in (Fig. 6a,b).

From Fig. 6, it can be noted that the designed structure achieves a polarization rotation bandwidth of 84%, ranging from 5.7 to 14 GHz, with a PCR exceeding 90%. Satisfactory agreement is obtained between simulation & measurement findings with some deviations at certain frequency points. Similar results are anticipated for 'x'-polarised incidence due to the symmetry of the structure.

RCS reduction with PCM

In order to observe the association between the PCR of the proposed PRRS and its effect in RCS reduction, we have computed the RCS of the structure, with respect to PEC surface of the same size[45].

$$\text{RCS (dB)} = 10log_{10}\left[\frac{\lim\limits_{R\to\infty} 4\pi R^2\left(\frac{|\overline{E_{ry}}|}{|\overline{E_{iy}}|}\right)^2}{\lim\limits_{R\to\infty} 4\pi R^2(1)^2}\right] = r_{yy}(dB) \tag{2}$$

Using (1) we can deduce,

$$\text{RCS} = 10\log(1 - \text{PCR}).$$

Now, a good RCS reduction over a wide frequency band is accomplished using a wideband PRRS with a high PCR value. It is clear that PRRS is only affecting a rotation of polarization and this power is scattered in

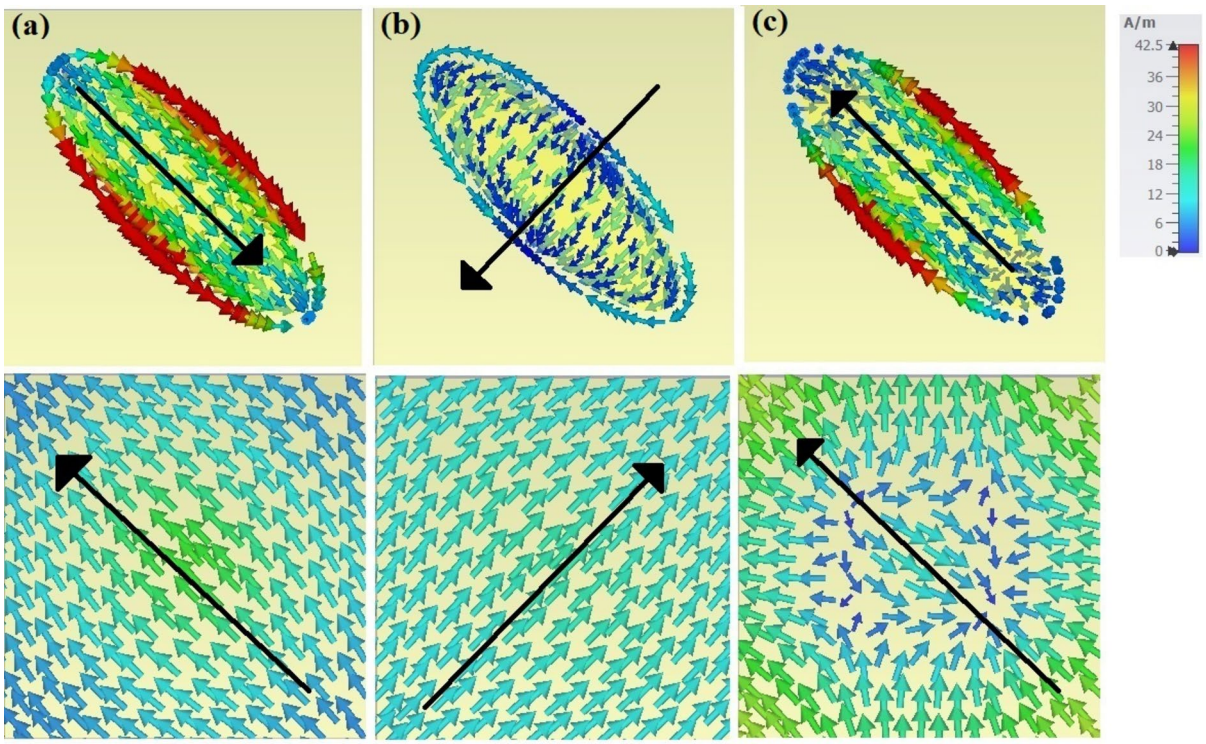

Fig. 4. Surface current patterns on unit cell at three resonating frequencies: (**a**) 6.8 GHz (**b**) 10.2 GHz, (**c**) 13.5 GHz.

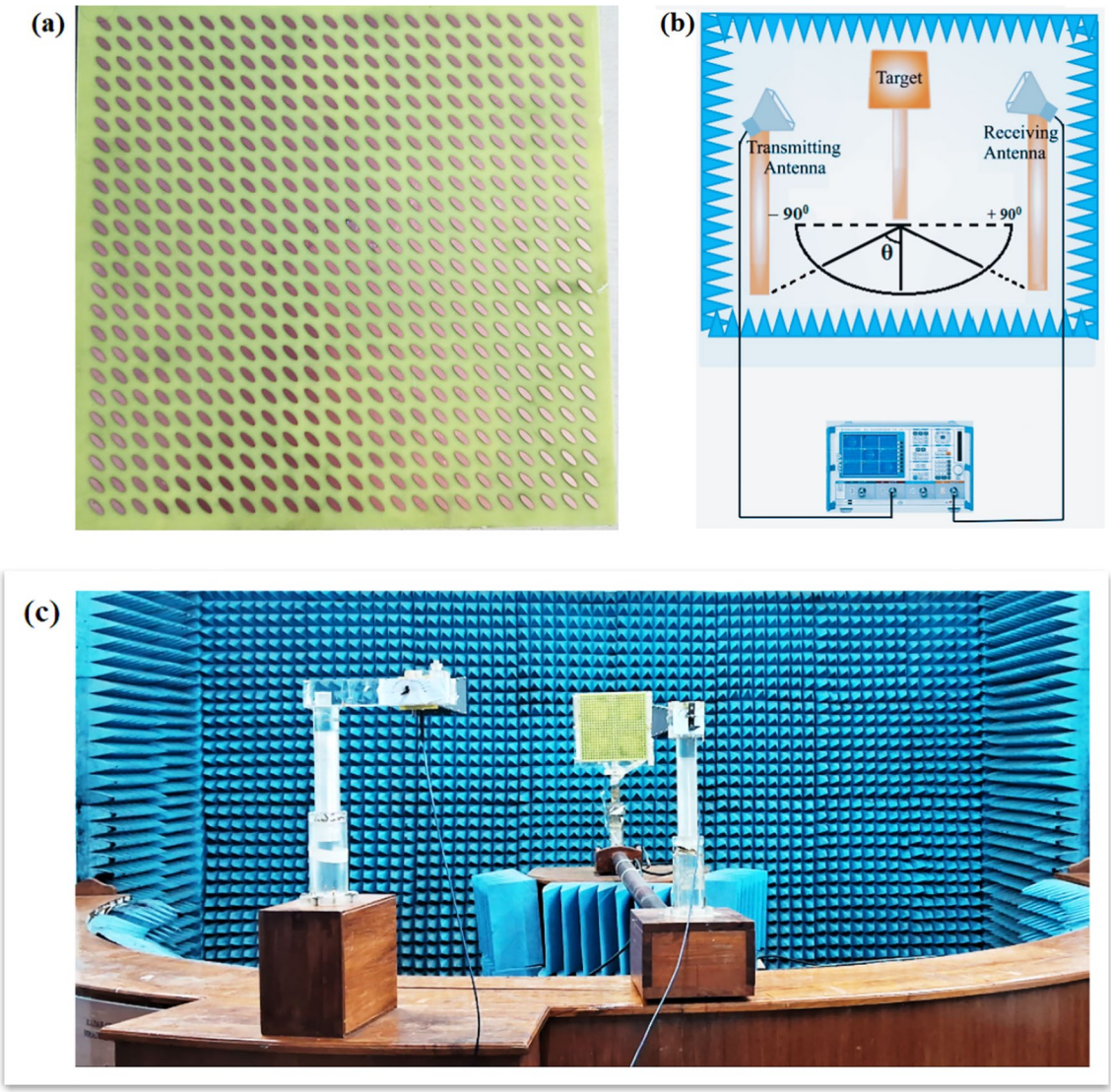

Fig. 5. (**a**) Fabricated prototype (**b**) Schematc diagram of the measurment setup (**c**) Measurement set up.

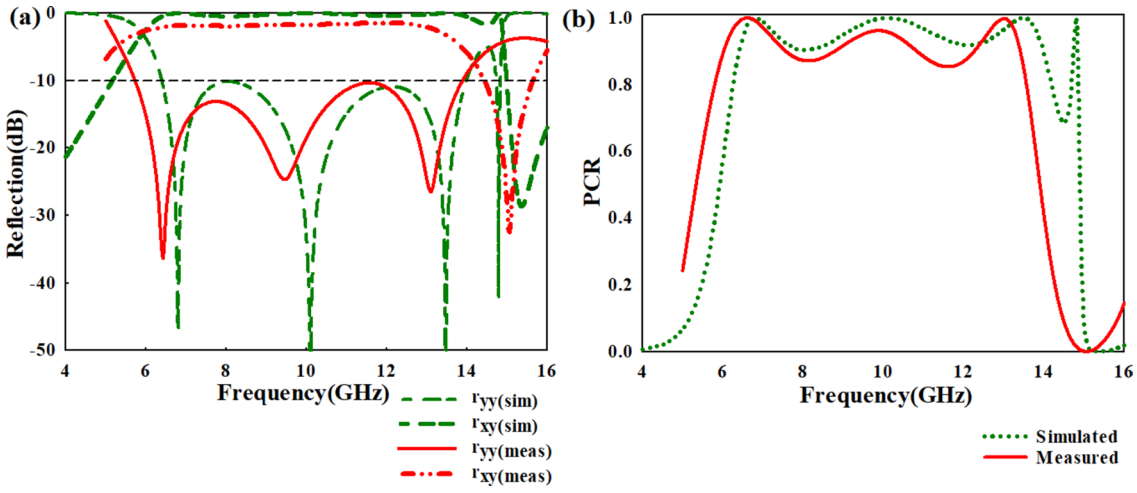

Fig. 6. Simulated & measured (**a**) co & cross-polarized reflection coefficients, and (**b**) PCR.

the incidental direction. As described in the Fig. 3a, b, two unit cells 90^0 to each other give the rotated field in opposite directions. No energy is scattered along the incident direction in the same polarization. Therefore, a checkerboard surface is formed by arranging the suggested unit cells in an orthogonal pattern. So that the rotated fields get cancelled in the incident direction.

A 24×24 array of PCM unit cells, along with their mirrors, is arranged in four sections, as portrayed in (Fig. 7). The fabricated prototype is depicted in (Fig. 7a). The simulated array in Fig. 7b illustrates the direction of the reflected electric field which aims to cancel the reflected electric field from various parts of the surface, leading to a remarkable dilution in RCS. Simulated & measured RCS normally incident for TE & TM waves is presented in (Fig. 7c). The chessboard arrangement using PRRS units attains an 84% bandwidth of 10 dB RCS reduction (5.7–14 GHz) in comparison to a metallic plate of same size. The structure effectively reduces RCS for both TE & TM polarised incidence waves, facilitated by mirrored ellipse unit cells across the 'X' and 'Y' axes. Overall, there is satisfactory agreement among simulation and measurement outcomes within the frequency band, with minor deviations.

Figure 8 displays 3D scattered pattern of the structure at 6.8 and 10 GHz, where RCS reduction is maximum. These visualizations illustrate how the surface alters the direction of the incoming wave and reduces RCS. The reflected waves from the surface divide into 4 segments at an elevation angle of $\theta = 20.8°$, with segments each at $\varphi = 45$, 135, 225, and 315°. Figure 9 shows the suggested metasurface achieves over 28 and 30 dB RCS reduction at the principal ($\varphi = 90°$) planes at 6.8 & 10 GHz, respectively, in comparison to the RCS of the metallic plate (maximum).

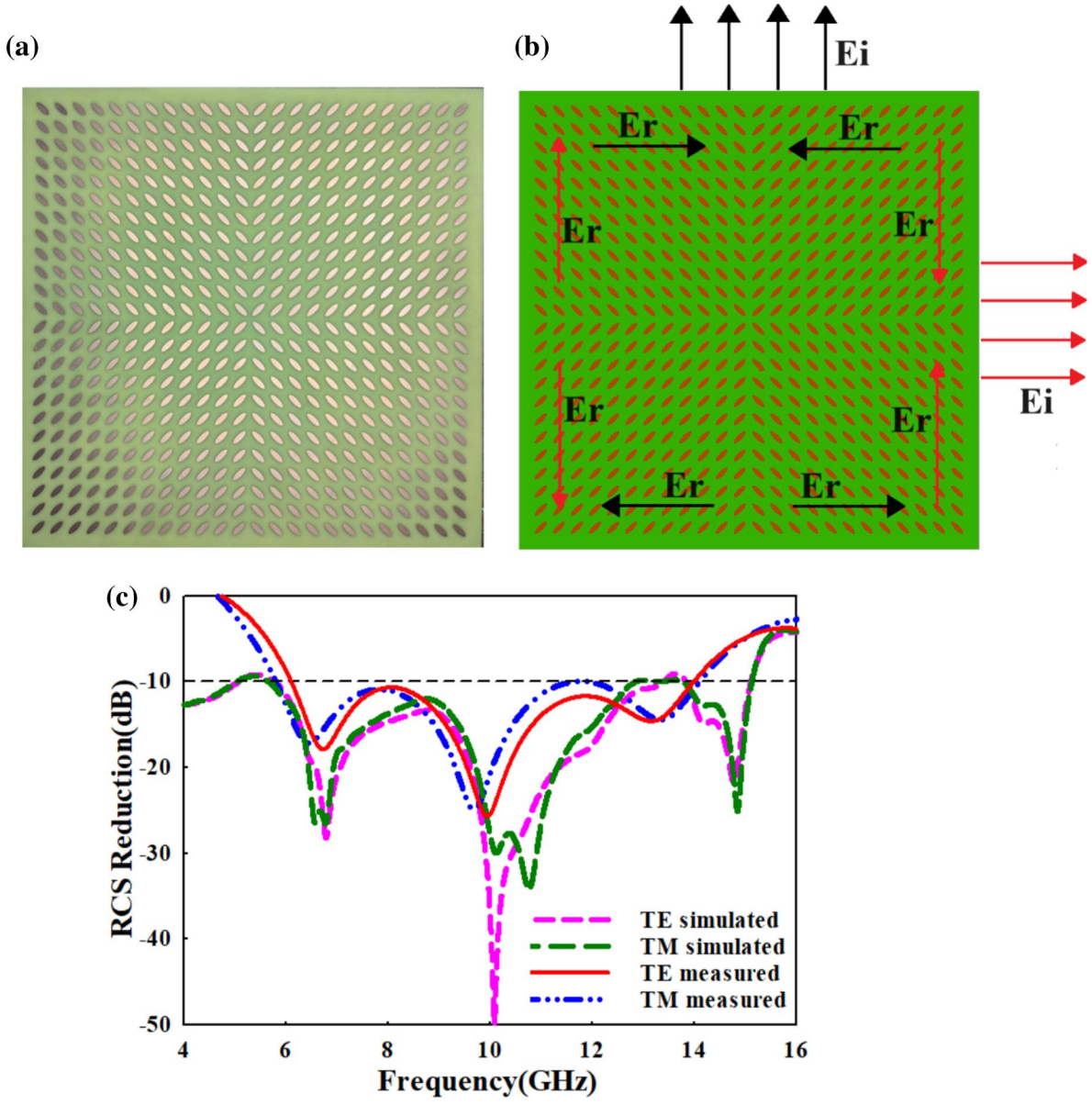

Fig. 7. (**a**) Fabricated prototype (**b**) Simulated array and (**c**) RCS reduction obtained.

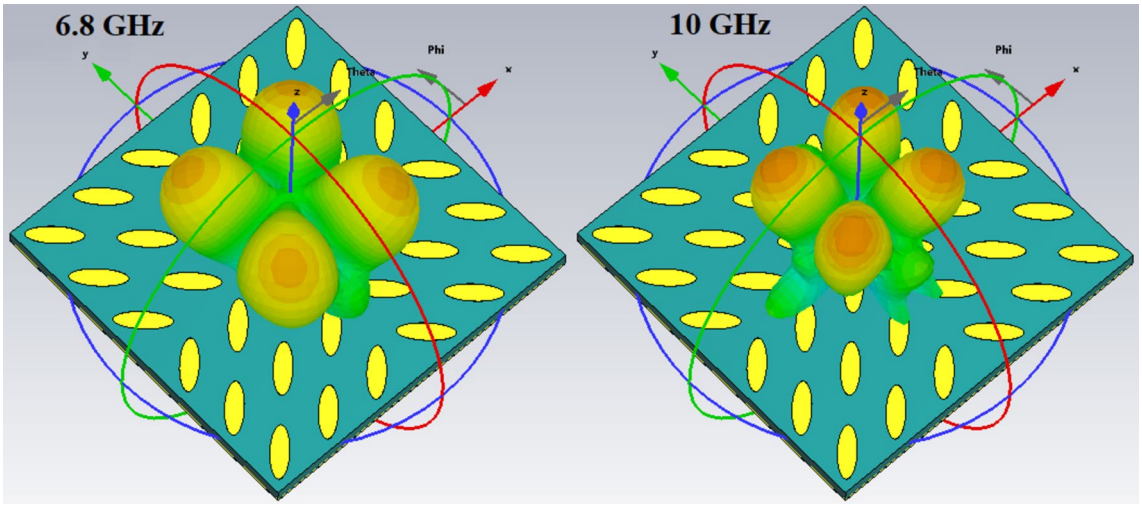

Fig. 8. 3D scattered fields at 6.8 and 10.8 GHz under normal incidence.

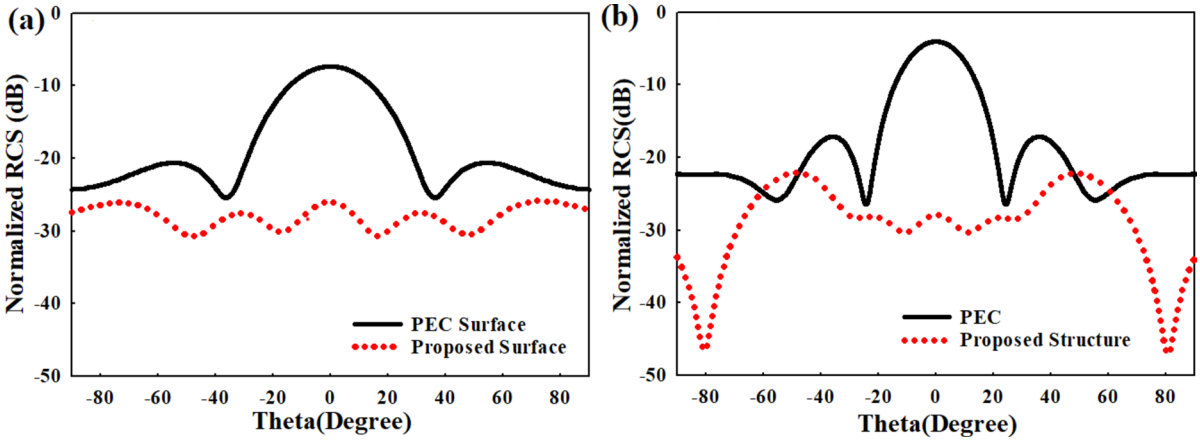

Fig. 9. Simulated RCS for the $\varphi = 0°$ ($\varphi = 90°$) plane compared with an equal-sized metallic plate (**a**) 6.8 GHz, and (**b**) 10 GHz.

Polarization insensitive RCS reduction

Since the unit cells are oriented in $45^0(135^0)$ the polarization rotation or RCS reduction is obtained for 0^0 and 90^0 incident polarizations only. For achieving polarization insensitivity specifically for reducing RCS, a new method is suggested. Instead of using a single-layer structure, another layer with unit cell arranged in different orientations is employed. The schematic of this double layer structure is depicted in (Fig. 10a). The bottom layer features vertically or horizontally etched ellipse structures with a ground on the backside, while the top layer is identical to that in (Fig. 6). The two layers are perfectly aligned and closely packed without any air gap between them. This configuration gives wideband RCS reduction where in the top and bottom layers with elliptical unit cells arranged in different orientations nullify the reflected waves towards the antenna, irrespective of the polarisation of the incident wave.

The structure's performance was evaluated using the same set up used earlier. The measured RCS reduction, compared to the simulations, is illustrated in the (Fig. 10b) The results indicate an RCS reduction bandwidth

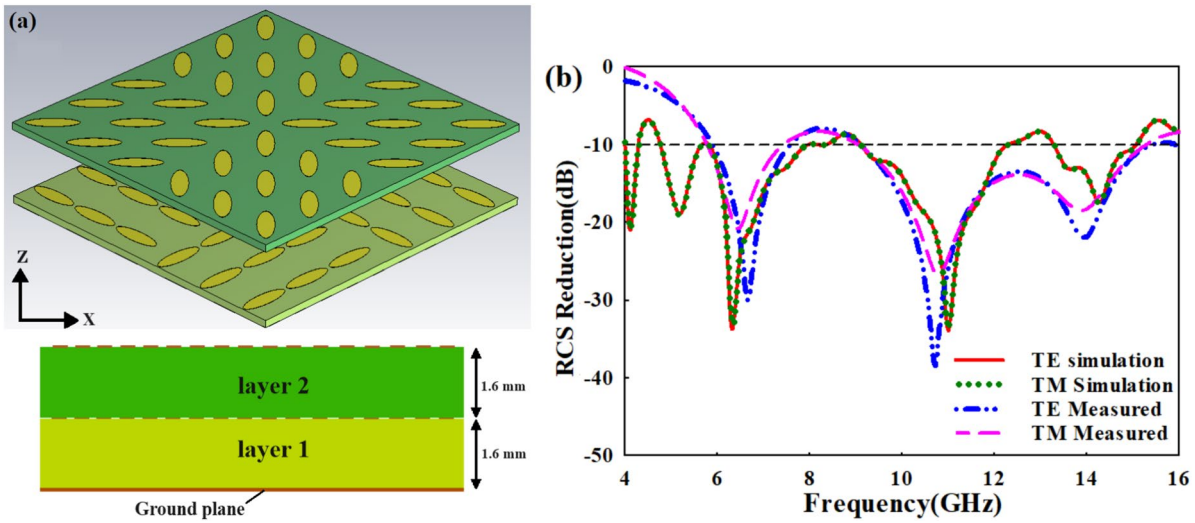

Fig. 10. (**a**) The proposed arrangement to achieve polarization-insensitive RCS reduction, and (**b**) Simulated and measured results for TE & TM modes.

of 90%, ranging from 5.8 to 15.3 GHz, for both TE & TM polarizations. Due to fabrication imperfections and measurement uncertainties, some deviations in the simulated and measured outcomes are observed.

So as to investigate the performance of the structure, the sample is fixed and measurement is taken with the receiving antenna rotated from a horizontal polarization ($\varphi = 0^0$) to a vertical polarization ($\varphi = 90^0$), for different incident polarizations(φ_i). The measured results for normal incidence for different polarisation are depicted in (Fig. 11a–f). The measured results demonstrate similar performance for all polarisation angles of EM wave incidence.

To find out the effect of angle of incidence on the RCS reduction property of the proposed structure, we studied bistatic RCS by varying incident angle(θ) from 0 to 45^0. The simulated result of the oblique incidence from 0^0 to 45^0 for both TE and TM polarization are shown in (Fig. 12a,b). The results show that wider incident angle stability is achieved. In order to verify the results experimentally, two standard horn antennas are used and the transmitting antenna is positioned for different incident angles from 0 to 45^0 on the arch set up measurement shown in (Fig. 5c). At each incident angle, the reflection from the structure was measured using a receiving horn antenna positioned at an angle to satisfy Snell's law. The measured results are depicted in the (Fig. 12c,d).

The performance of the proposed design is compared to similar designs previously documented, as depicted in (Table 1). The proposed design showcases consistent and better performance in terms of bandwidth, insensitivity to polarization, compactness and response to oblique incidence in comparison with other reported designs.

Conclusion

This paper proposes a new technique for reducing the RCS over a wide frequency range, while being insensitive to the incident angle and polarization to a large extent. Initially, a surface formed of an ellipse-shaped unit cell and its mirror image, helps decrease RCS over a wide bandwidth of 84%. However, this design is sensitive to incident polarization. To address this, a double-layer structure is used, with each layer forming a checkerboard surface with different orientations of ellipse structures. This approach achieves good RCS reduction over a wide frequency range, which remains almost constant under changes in polarization and incident angles. The measured results confirm that the structure is insensitive to polarization angles ranging from 0 to 90° and incident angles up to 45^0. This property of the proposed compact structure make it ideal for reducing RCS in stealth techniques and other similar applications.

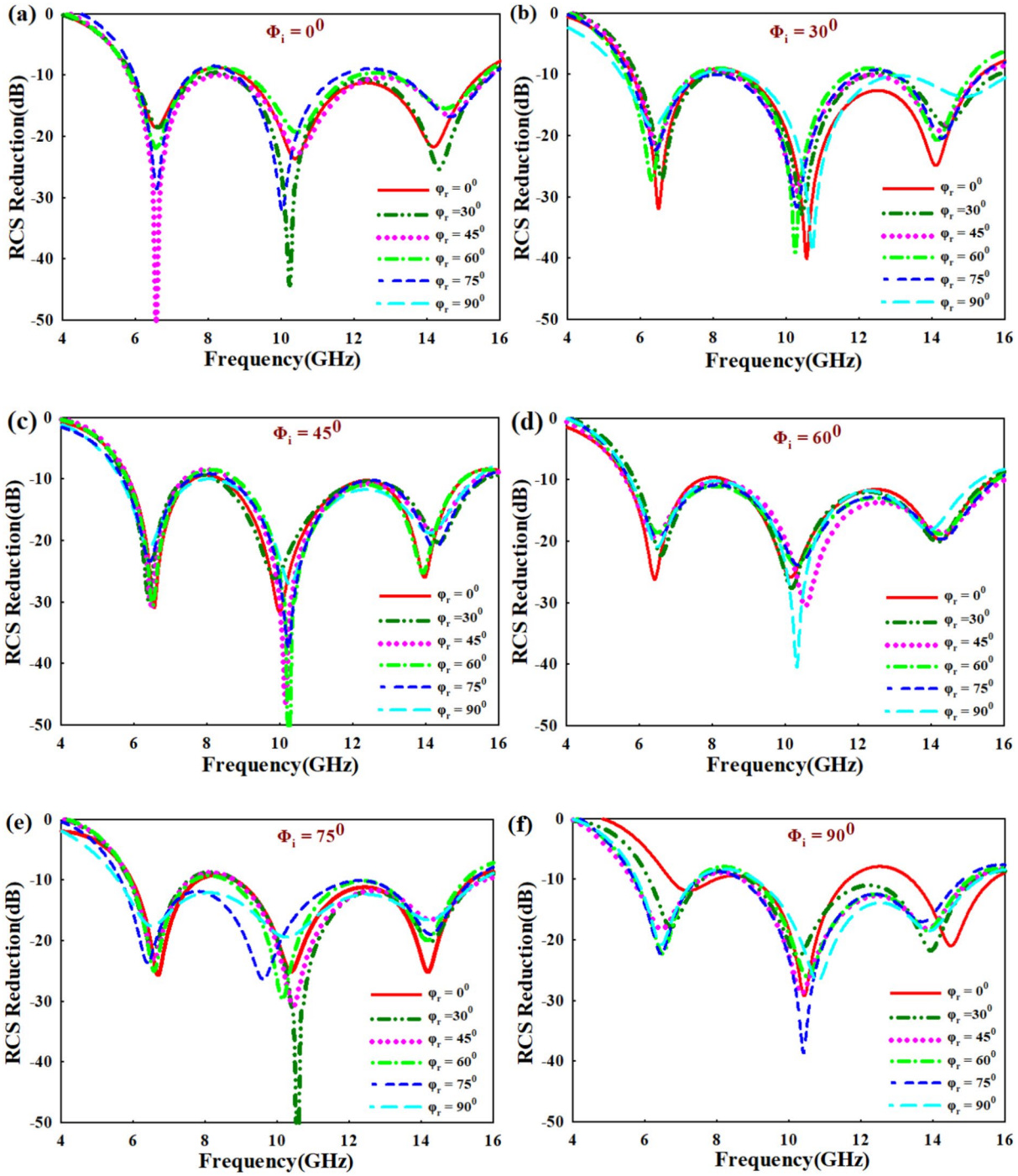

Fig. 11. RCS reduction curve at different polarization angles under various incident polarizations (**a**) 0° (**b**) 30° (**c**) 45^0 (**d**) 60^0 (**e**) 75^0 (**f**) 90^0.

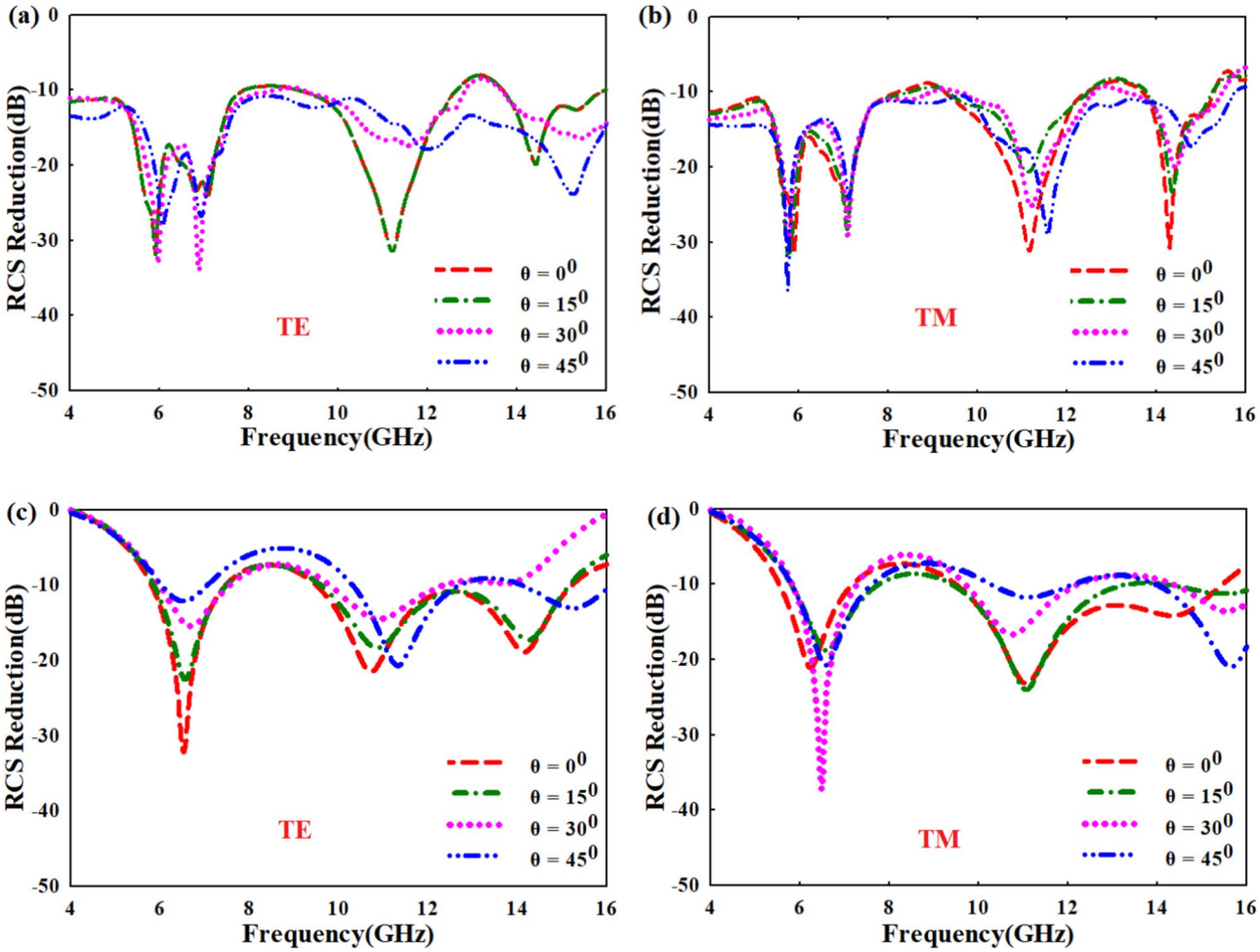

Fig. 12. RCS reduction values for different incident angles (**a**,**b**) simulated, (**c**,**d**) measured.

Ref	Substrate material	Symmetricity	-10 dB RCS reduction bandwidth	Thickness (mm)	Incidence angle insensitivity	Polarization angle insensitivity
[36]	FR4	Twofold symmetry	Not tested	3 mm	$\leq 30^0$	Polarization selective
[39]	F4B & curing film	Fourfold symmetry	Not checked	4.16 mm	Not shown	$0 \leq 90^0$
[40]	F4B-2 woven glass	Four fold symmetry	80.7% (17–42 GHz)	1.5	$0 \leq 40^0$	Not tested
[41]	Ordinary glass	Four fold symmetry	62% (18–34 GHz)	1.1	$\leq 45^0$	Not tested
[46]	FR4	Four fold symmetry	52%(7–12 GHz)	3	$0 \leq 30^0$	Not tested
[47]	F4B	Four fold symmetry	76.9(8–18 GHz)	3	$0 \leq 30^0$	Only tested for x and y polarization
[48]	RTduroid 5880	Four fold symmetry	129% (11.3–51.7 GHz)***RCS -7 dB***	1.6	$0 \leq 40^0$	$\leq 90^0$
Proposed	FR4	Two fold symmetry	91% (5.7–15.3 GHz)	3.2 mm	$\leq 45^0$	$\leq 90^0$

Table 1. Performance compared to other polarization insensitive structures.

Data availability

All data generated or analysed during this study are included in this article.

Received: 30 May 2024; Accepted: 9 September 2024
Published online: 20 September 2024

References

1. Knott, E. F., Schaeffer, J. F. & Tulley, M. T. *Radar Cross Section* (SciTech Publishing, 1993).
2. Smith, D. R., Padilla, W. J., Vier, D. C., Nemat-Nasser, S. C. & Schultz, S. Composite medium with simultaneously negative permeability and permittivity. *Phys. Rev. Lett.* **84**, 4184–4187 (2000).

3. Mei, Z., Ma, X., Lu, C. & Zhao, Y. High-efficiency and wide-bandwidth linear polarization converter based on double U-shaped metasurface. *AIP Adv.* **7**, 125323 (2017).
4. Rin, Xu., Li, R., Qin, J., Wang, S. & Han, T. Ultra-broadband wide-angle linear polarization converter based on H-shaped metasurface. *Opt. Express* **26**, 20913–20919 (2018).
5. Yu-Zhou, R. *et al.* Ultra-wideband linear-to-circular polarization converter with ellipse-shaped metasurfaces. *Opt. Commun.* **451**, 124–128 (2019).
6. Deng, Z. H., Wang, F. W., Ren, Y. H., Li, K. & Gao, B. J. A novel wideband low-RCS reflector by hexagon polarization rotation surfaces. *IEEE Access* **7**, 131527–131533 (2019).
7. Guo, L., Li, S., Jiang, X., Peng, L. & Li, X. Ultra-wideband polarization rotation reflective metasurface based on monolayer rhombus hollow structure. *AIP Adv.* **8**, 095205 (2018).
8. Cerveny, M., Ford, K. & Tennant, A. Reflective switchable polarization rotator based on metasurface with PIN diodes. *IEEE Trans. Antennas Propagat.* **69**, 1483–1492 (2021).
9. Liu, Y. *et al.* Wideband RCS reduction of a slot array antenna using polarization conversion metasurfaces. *IEEE Trans. Antennas Propagat.* **64**, 326–331 (2016).
10. Long, M., Jiang, W. & Gong, S. Wideband RCS reduction using polarization conversion metasurface and partially reflecting surface. *IEEE Antennas Wirel. Propagat. Lett.* **16**, 2534–2537 (2017).
11. Zheng, Y. *et al.* Ultra-wideband polarization conversion metasurface and its application cases for antenna radiation enhancement and scattering suppression. *Sci. Rep.* **7**, 16137 (2017).
12. Anand, S. Planar polarization rotation reflective surface for X-band RCS reduction in microstrip patch antenna. *E-Prime Adv. Elect. Eng. Electron. Energy* **4**, 100164 (2023).
13. Jia, Y., Liu, Y., Guo, Y., Li, K. & Gong, S. X. Broadband polarization rotation reflective surfaces and their applications to RCS reduction. *IEEE Trans. Antennas Propagat.* **64**, 179–188 (2016).
14. Yang, J. J., Cheng, Y. Z., Ge, C. C. & Gong, R. Z. Broadband polarization conversion metasurface based on metal cut-wire structure for radar cross section reduction. *Materials* **11**, 626 (2018).
15. Zaker, R. & Sadeghzadeh, A. A low-profile design of polarization rotation reflective surface for wideband RCS reduction. *IEEE Antennas Wirel. Propagat. Lett.* **18**, 1794–1798 (2019).
16. Chen, W., Shi, J., Niu, Z., & Gu, C. Broadband Polarization Conversion Metasurface for Radar Cross Section Reduction. *International Conference on Microwave and Millimeter Wave Technology (ICMMT)*. 1–3 (2018).
17. Jia, Y., Liu, Y., Guo, Y., Li, K. & Gong, S. A Dual-Patch Polarization Rotation Reflective Surface and Its Application to Ultra-Wideband RCS Reduction. *IEEE Trans. on Antennas and Propagat* **65**, 3291–3295 (2017).
18. Zheng, Q., Guo, C., Li, H. & Ding, J. Broadband radar cross-section reduction using polarization conversion metasurface. *Int. J. Microw. Wirel. Technol.* **10**, 197–206 (2018).
19. Zhen, Q. *et al.* RCS reduction effect based on transparent and flexible polarization conversion metasurface arrays. *Results Phys.* **52**, 106886 (2023).
20. Ameri, E., Esmaeli, S. & Sedighy, S. Ultra wideband radar cross section reduction by using polarization conversion metasurfaces. *Sci. Rep.* **9**, 478 (2019).
21. Modi, A., Balanis, C., & Birtcher, C. Novel technique for enhancing RCS reduction bandwidth of checkerboard surfaces. *IEEE International Symposium on Antennas and Propagation & USNC/URSI National Radio Science Meeting*. 1911–1912 (2017).
22. Sang, D., Chen, Q., Ding, L., Guo, M. & Fu, Y. Design of checkerboard amc structure for wideband RCS reduction. *IEEE Trans. Antennas Propagat.* **67**, 2604–2612 (2019).
23. Zhuang, Y. Q., Wang, G. M. & He-Xiu, Xu. Ultra-wideband RCS reduction using novel configured chessboard metasurface*. *Chin. Phys. B* **26**, 054101 (2017).
24. Mol, V. L. & Aanandan, C. Wideband radar cross section reduction using artificial magnetic conductor checkerboard surface. *Progress Electromagnet. Res. M* **69**, 171–183 (2018).
25. Ameri, E., Esmaeli, S. H. & Sedighy, S. H. Ultra wide band radar cross section reduction using multilayer artificial magnetic conductor metasurface. *J. Phys. D Appl. Phys/* **51**, 285304 (2018).
26. Iriarte, J. *et al.* Broadband radar cross-section reduction using AMC technology. *IEEE Trans. Antennas Propagat.* **61**, 6136–6143 (2013).
27. Ali, L., Li, Q., Khan, T. A., Yi, J. & Chen, X. Wideband RCS reduction using coding diffusion metasurface. *Materials* **12**, 2708 (2019).
28. Zhang, G., Sui, S., Wang, A., Wang, J., Qu, S., & Wang, J.Coding Metasurface for Radar Cross Section Reduction. *IEEE 3rd International Conference of Safe Production and Informatization (IICSPI)*. 52–55 (2020).
29. Ramachandran, T. *et al.* Development of diverse coding metamaterial structure for radar cross section reduction applications. *Sci. Rep.* **12**, 10958 (2022).
30. Sun, H. *et al.* Broadband and Broad-angle polarization-independent metasurface for radar cross section reduction. *Sci. Rep.* **7**, 40782 (2016).
31. Ren, Z. *et al.* Ultra-broadband RCS reduction based on optimized coding "whale-shaped" polarization conversion metasurface with angular stability. *IEEE Access* **10**, 50479–50486 (2022).
32. Akbari Choubar, M., Samadi, F., Sebak, A. & Denidni, T. Superbroadband diffuse wave scattering based on coding metasurfaces. *IEEE Antennas Propagat. Mag.* **61**, 40–52 (2019).
33. Li, S. *et al.* Ultra-broadband reflective metamaterial with RCS reduction based on polarization convertor, information entropy theory and genetic optimization algorithm. *Sci. Rep.* **6**, 37409 (2016).
34. Deng, G. Y. *et al.* Ultra broadband RCS reduction design by exploiting characteristic complementary polarization conversion metasurfaces. *IEEE Trans. Antennas Propagat.* **70**, 2904–2914 (2022).
35. Chatterjee, J., Mohan, A. & Dixit, V. Ultrawideband RCS reduction of planar and conformal surfaces using ultrathin polarization conversion metasurface. *IEEE Access* **10**, 36563–36575 (2022).
36. Yin, *et al.* Ultra wideband polarization-selective conversions of electromagnetic waves by metasurface under large-range incident angles. *Sci. Rep.* **5**, 12476 (2015).
37. Khan, M., Fraz, Q. & Tahir, F. Ultra-wideband cross polarization conversion metasurface insensitive to incidence angle. *J. Appl. Phys.* **121**, 045103 (2017).
38. Jinghong, Wu. *et al.* A wide-incidence-angle insensitive multi-polarization converter based on reflective metasurface. *J. Phys. D Appl. Phys.* **56**, 415103 (2023).
39. Liu, W. *et al.* Metasurface-based broadband polarization-insensitive polarization rotator. *Opt. Express* **30**, 34645–34654 (2022).
40. Sun, H. *et al.* Broadband and broad-angle polarization-independent metasurface for radar cross section reduction. *Sci. Rep.* **7**, 40782 (2017).
41. He, X., Qi, C. & Wong, A. M. A compact transparent polarization-insensitive metasurface with broadband monostatic and bistatic radar cross-section reduction of millimeter-waves. *J. Phys. D Appl. Phys.* **55**, 355104 (2022).
42. Jia, Y., Liu, Y., Guo, Y., Li, K. & Gong, S. A dual-patch polarization rotation reflective surface and its application to ultra-wideband RCS reduction. *IEEE Trans. Antennas Propagat.* **65**, 3291–3295 (2017).
43. Indhu, K. K. *et al.* Low profile wideband polarization rotation reflective metasurface. *Progress Electromagnet. Res. C* **137**, 39–51 (2023).

44. Gao, X. *et al.* Ultrawideband and high-efficiency linear polarization converter based on double V-shaped metasurface. *IEEE Trans. Antennas Propagat.* **63**, 3522–3530 (2015).
45. Jia, Y., Liu, Y., Guo, Y. J., Li, K. & Gong, S. Broadband polarization rotation reflective surfaces and their application to RCS reduction. *IEEE Trans. Antenn. Propag.* **64**, 179–188 (2016).
46. Song, Y. C., Ding, J., Guo, C. J., Ren, Y. H. & Zhang, J. K. Ultra-broadband backscatter radar cross section reduction based on polarization-insensitive metasurface. *IEEE Antennas Wirel. Propagat. Lett.* **15**, 329–331 (2016).
47. Su, P. *et al.* An ultra-wideband and polarization-independent metasurface for RCS reduction. *Sci. Rep.* **6**, 20387 (2016).
48. Su, J. *et al.* Ultra-wideband, wide angle and polarization-insensitive specular reflection reduction by metasurface based on parameter-adjustable meta-atoms. *Sci. Rep.* **7**, 42283 (2017).
49. Fathnan, A. A. & Powell, D. A. Bandwidth and size limits of achromatic printed-circuit metasurfaces. *Opt. Express* **26**, 29440–29450 (2018).
50. Hayran, Z. & Monticone, F. Beyond the rozanov bound on electromagnetic absorption via periodic temporal modulations. *Phys. Rev. Appl.* **21**, 044007 (2024).

Author contributions

Indhu K. K. did the major part of the work including the conceptualisation, design and simulation of the structure. Abhilash A P and Anilkumar R participated in the fabrication, measurement and analysis. Deepti Das K and Aanandan C K did the supervision, technical guidance, editing and review.

Competing interests

The authors declare no competing interests.

Additional information

Correspondence and requests for materials should be addressed to K.K.I.

Reprints and permissions information is available at www.nature.com/reprints.

Publisher's note Springer Nature remains neutral with regard to jurisdictional claims in published maps and institutional affiliations.